

LDA + DMFT study of Ru-based perovskite SrRuO₃ and CaRuO₃

E. Jakobi,¹ S. Kanungo,² S. Sarkar,² S. Schmitt,³ and T. Saha-Dasgupta²

¹*Institute of Physics, Johannes Gutenberg University, 55099 Mainz, Germany*

²*S. N. Bose Centre for Basic Sciences, Kolkata 700 098, India*

³*Technische Universität Dortmund, DE-44221 Dortmund, Germany*

(Received 8 October 2010; published 11 January 2011)

We carried out a LDA + DMFT study of perovskite ruthenates SrRuO₃ and CaRuO₃, compounds which have been discussed in great detail in recent literature. Our results reproduced the observed mass enhancements and magnetic properties, and were in reasonable agreement with the measured photoemission spectra. Our calculations produced rather different coherence temperatures for SrRuO₃ and CaRuO₃, providing a possible explanation for the observed differences between these compounds. We also present **k**-resolved spectra for the sake of comparison with future angle-resolved photoemission experiments.

DOI: [10.1103/PhysRevB.83.041103](https://doi.org/10.1103/PhysRevB.83.041103)

PACS number(s): 71.20.Be, 71.27.+a, 71.15.Ap

I. INTRODUCTION

The correlated electron systems of transition metal (TM) oxides have been a constant focus for researchers. A pertinent question in this context has been how the electron-electron correlation behaves as one moves down the periodic table from 3d to 4d to 5d TM oxides. Compounds that have been discussed most in this context are 4d Ru-based perovskites SrRuO₃ (SRO) and CaRuO₃ (CRO). While SRO is a ferromagnetic metal with a Curie temperature (T_c) of about 160 K,¹ CRO does not show any magnetic ordering though it remains metallic.² The nature of the metallic state remains controversial. A number of experimental studies have been carried out employing various possible tools, such as x-ray and ultraviolet photoemission spectroscopy (PES),^{3,4} specific-heat measurements,⁵ transport measurements,¹ and optical-conductivity measurements.⁶ While all the experimental results point to some role of electron-electron correlation, the strength and the extent of its importance still remain debatable and unclear. On the theoretical front, calculations have been carried out within the framework of the local density approximation (LDA) and its extensions, such as the generalized gradient approximation (GGA).⁷ In order to take into account correlations beyond LDA and GGA, calculations have been carried out within the framework of LDA + U as well as the self-interaction correction (SIC).^{8,9} While such approaches, which incorporate static correlation effects, are appropriate for dealing with insulators, because SRO and CRO are metals, the dynamical effects are expected to be crucial for a proper description. For example, the LDA + U with $U > 2$ eV predicts a half-metallic ground state with orbital ordering for SRO, which is not observed experimentally. Given the available tools to deal with correlation effects, the dynamical mean field theory (DMFT),¹⁰ therefore, appears to be the natural choice to describe these ruthenates. In combination with LDA, the so-called LDA + DMFT approach is expected to capture the material-specific differences between SRO and CRO correctly, including correlation effects.

In this work, we present the electronic-structure calculation of SRO and CRO within the framework of LDA + DMFT, which to the best of our knowledge has not been attempted before. Our results show both SRO and CRO to be moderately correlated. With a choice of U value we could reproduce the

mass renormalizations as well as their ratios between Sr and Ca compounds in reasonable agreement with that observed in the optical experiment.⁶ The U value fixed by consideration of mass renormalization gave rise to a ferromagnetic (FM) solution for SRO and a solution with no magnetic ordering in the case of CRO. The computed FM moment for SRO is found to be in reasonable agreement with the experimental measurements. The computed **k**-integrated spectral function is found to reproduce the primary features of PES data. We found the coherence temperature for SRO to be substantially higher than that for CRO, providing a possible explanation for the observed non-Fermi-liquid (FL) behavior in one case and not in the other. Additionally, we computed the **k**-resolved spectral function, which can be compared with future angle-resolved PES (ARPES) experiments.

Both SRO and CRO crystallize in a four-formula-unit (f.u.) orthorhombic perovskite structure (ABO₃) exhibiting a GdFeO₃ kind of distortion associated with rotation and tilt of RuO₆ octahedra. For SRO, this leads¹¹ to an Ru-O-Ru in-plane angle of 161.1° and an Ru-O-Ru out-of-plane angle of 164.9°. Replacement of the Sr ion by a Ca ion reduces the size of the A cation and modifies the A-O covalency,¹² leading to further reduction¹³ of the in-plane Ru-O-Ru angle to 151.1° and the out-of-plane Ru-O-Ru angle to 137.6°. The well-studied⁷ LDA electronic structure of SRO, as presented in Fig. 1, consists of an O- p -Ru- d hybridized band structure that extends from about -8 eV below the Fermi level (E_f) to about 6 eV above E_f . The empty Sr bands lie higher up, above 6 eV. The Ru- d -dominated states, separated by a dip-like feature from O- p -dominated states in the density of states (DOS), give rise to a d -band width of about 8.5 eV. Replacement of Sr by Ca, causing a reduction of the Ru-O-Ru angle, results in a clear gap between O- p -dominated states and Ru- d -dominated states as well as a reduction of width associated with Ru- d -dominated states to about 7.5 eV. The octahedral surrounding of Ru splits the Ru- d complex into t_{2g} and e_g levels. Ru, which is normally in a low-spin, d^4 configuration, gives rise to a $t_{2g}^3 \uparrow t_{2g}^1 \downarrow$ configuration with E_f lying in the t_{2g} manifold with empty e_g states. In order to interface with the DMFT calculation, starting from such all-band LDA descriptions, we employed the N^{th} -order muffin-tin orbital (NMO) based downfolding method,¹⁴ which reduces the

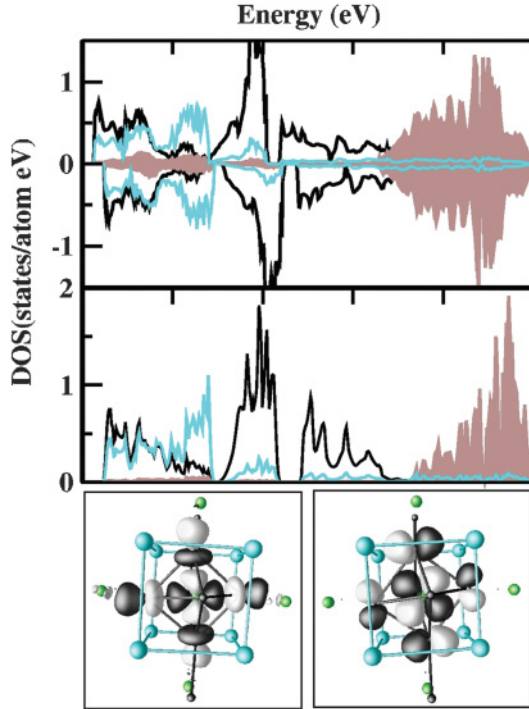


FIG. 1. (Color online) Top panels: LDA density of states of SRO (upper panel) and CRO (lower panel). The DOS projected onto O- p , Ru- d , and Sr/Ca- d are shown with cyan (light gray), black, and shaded lines. For CRO this leads to a nonmagnetic solution with identical DOS between spin-up and spin-down channels. The bottom panel shows the effective Wannier functions corresponding to Ru- d_{xy} (left) and Ru- $d_{x^2-y^2}$ (right) for SRO. Plotted are the orbital shapes (constant-amplitude surfaces) with lobes of opposite signs colored black and white.

all-band Hamiltonian to a low-energy, few-band Hamiltonian described on an effective Wannier-function basis. This is achieved by integrating out the degrees of freedom that are not of interest. For the present study, we kept active Ru- d orbitals, including both t_{2g} and e_g , and integrated out all the rest involving O and Sr degrees of freedom. This defines the effective Ru t_{2g} and e_g Wannier functions. The representative functions are shown in the bottom panel of Fig. 1. The central parts of the Wannier functions are shaped according to the symmetry of atomic Ru- d orbitals, while the tails sitting at the O or A site are shaped according to O- p or Sr/Ca symmetries.

The multiorbital Hubbard model defined on the basis of NMTO-downfolding constructed Ru- d Wannier functions is given by $H = H_{\text{LDA}} + \frac{1}{2} \sum_{i,mnop\sigma\sigma'} \hat{c}_{im\sigma}^\dagger \hat{c}_{i\sigma'}^\dagger \hat{c}_{i\sigma} \hat{c}_{ip\sigma'} U_{mnop}$, with \hat{c}_x^\dagger and \hat{c}_x defined as creation and annihilation operators, respectively. The atomic sites (Ru-only sublattice) are denoted by indices i ; the orbital indices m, n, \dots run over five d orbitals of Ru, and σ, σ' are spin indices. U_{mnop} are the Slater integrals. Within spherical symmetry these are connected to the Slater-Condon parameters,¹⁵ expressed via the well-known relations $U = F^{(0)}$ and $J = \frac{1}{14}[F^{(2)} + F^{(4)}]$, with $F^{(2)}/F^{(4)}$ approximately constant. In this work we restrict ourselves to the choice¹⁶ $J = U/2$.

Starting from the LDA inputs, this multiorbital Hubbard Hamiltonian was subsequently solved by employing the DMFT. The associated impurity model of the DMFT was solved using a diagrammatic weak-coupling solver up to second order. The current approach¹⁷ originates conceptually from iterative perturbation theory (IPT) and reduces in the single-band case to the initial IPT ansatz.¹⁸ However, the multiband scenario, as in the present case, is different from other extensions of IPT approaches such as that of Kajueter *et al.*,¹⁹ which is done on the basis of a single diagram or a few diagrams. In a multiband situation, the electron in a particular orbital in principle can scatter from all the orbitals, involving all the atoms in the unit cell, which in the present case is 20, considering 4 Ru atoms in the unit cell and 5 d orbitals per Ru atom. This is modeled rigorously within the current approach by collecting all possible scattering processes up to second order. Corrections to first order are ignored, assuming that corrections to the static Hartree and Fock diagrams are globally compensated by the chemical potential. This leads to the generation of approximately 130 000 diagrams for the present problem. The advantage of this procedure is that the diagrams can be calculated at the real-frequency axis by consecutive convolutions. Therefore, the Green functions and spectral functions can be directly evaluated at the real-frequency axis, in contrast to impurity solvers like quantum Monte Carlo (QMC). In order to investigate the temperature effect, one needs to be below the magnetic-ordering temperature of SRO, which is 160 K. Most of the results presented in the manuscript have been carried out down to a temperature of 73 K. With four atoms per unit cell and five orbitals per atom, reaching such a low temperature with a QMC approach is prohibitively expensive, scaling with the temperature (T) as $1/T^3$ and with the number of involved orbitals (m) as m^2 . The disadvantage of the present approach, however, is the weak-coupling approach itself. This approach may be applied only in situations where the bandwidths are large compared to the interaction integrals. Considering the present case of ruthenates with rather large effective bandwidths of ≈ 8 eV, such an approach is a viable one. The reasonable agreement between calculated properties such as magnetic moment, the mass enhancement, photoemission spectra, and the experimental measurements, as presented in the following, support the validity of the present approach.

Since the strength of the interaction is not quite known and has been a source of debate, we varied U over a range of values. Fig. 2(a) shows the plot of calculated mass-enhancement factor related to quasiparticle spectral weight Z and the real part of self-energy, Σ , as $m^* = 1/Z = (1 - \partial \text{Re} \Sigma / \partial \omega)$ for the Sr compound as well as for the Ca compound. We find that, as expected, m^* increases as U increases. For a choice of U value of about 3.5 eV, the mass enhancement for SRO turns out to be about 2.5. Considering the contribution from only t_{2g} degrees of freedom, the relevant one with a d^4 low-spin configuration, m^* for SRO is about 3, while that for CRO is about a factor of 1.4–1.5 larger. The results are in reasonable agreement with those obtained from optical conductivity measurements.⁶ We note that for smaller values of U close to 1 eV or so, as predicted by LDA + U or SIC calculations,⁸ we are unable to reproduce the observed mass enhancement and the relative ratio of mass enhancement between the Sr and the Ca compound. The

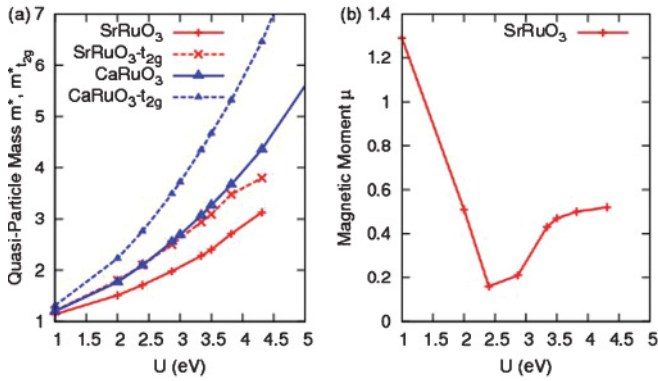


FIG. 2. (Color online) (a) Mass enhancement obtained in LDA + DMFT calculations for SRO and CRO. (b) FM moment of SRO plotted as a function of strength of electron-electron correlation, U . Panel (b) also shows the unscreened local moments for SRO and CRO.

LDA + DMFT calculations for the Sr compound resulted in a ferromagnetically ordered solution, while CRO did not order. The FM moment for the SRO compound as a function of varying U , as presented in Fig. 2(b), shows an interesting variation. As the value of U is increased, the net magnetic moment decreases due to transfer of spectral weight from up-spin channel to down-spin channel until it hits a minimum for a U value of about 2.5 eV, where the populations of the two spin channels become nearly equal. Increasing the U value further causes population reversal, leading to an increase in net magnetic moment. The U value chosen from consideration of the mass renormalization (3.5 eV) gave rise to a magnetic moment of about $0.5\mu_B$. The measured value²⁰ of the saturation moment shows a rather wide variation, from 0.9 to $1.5\mu_B$. Keeping in mind that the present LDA + DMFT calculation implemented in the basis of effective Ru- d Wannier function gives only the magnetic moment at the Ru site and that the large Ru-O covalency leads to substantial moments sitting at O sites, the obtained magnetic moment may not be an unreasonable estimate. Considering the LDA estimates of magnetic moment at O sites ($\approx 0.5\mu_B$ per f.u.) and assuming the correlation-driven renormalization for oxygen states to be small, this would amount to a total magnetic moment of about $1.0\mu_B$ per f.u. In comparison to the ordered moment we also present the unscreened moments of the Ca and Sr compounds in Fig. 2(b). This is determined by the probability of finding the Ru orbitals in the singly occupied configuration, as compared to empty and doubly occupied ones, and is nonzero also for the nonmagnetic CRO. While both have the same order of magnitude, the SRO unscreened moment is somewhat larger owing to the FM polarization.

In Figs. 3(a) and 3(c) we present the LDA + DMFT spectral functions plotted in comparison to the downfolded LDA density of states in the effective Ru- d bases for SRO and CRO. The U was chosen to be 3.5 eV, while T was set at 73 K. The redistribution of spectral weight and the formation of Hubbard-like subbands upon application of the correlation effect is clearly visible. In Fig. 3(b), we present the comparison of the spin-integrated LDA + DMFT spectra for SRO with photoemission data reproduced from Ref. 3. For comparison we also present the spin-integrated downfolded LDA DOS. We

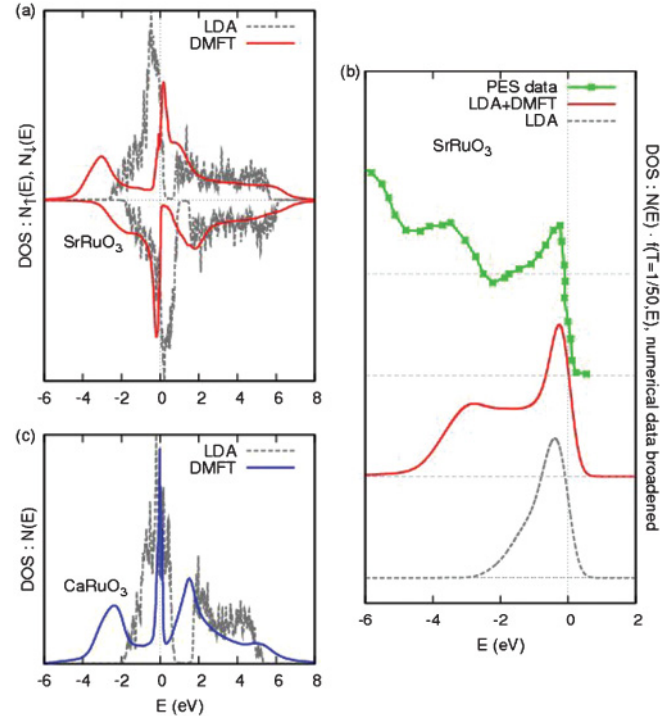


FIG. 3. (Color online) LDA + DMFT spectral functions of (a) SRO and (c) CRO in comparison with LDA DOS. Only one of the spin channels is plotted for CRO since there is no net magnetic moment. (b) The spin-integrated LDA + DMFT spectral function and LDA DOS of SRO in comparison with photoemission data from Ref. 3. The LDA + DMFT and LDA spectra are broadened by a Gaussian function with a full width at a half maximum of 0.25 eV to account for the instrumental broadening.

find that the LDA + DMFT spectral function reproduces the sharp quasiparticle peak, the dip, followed by a hump obtained from a Hubbard subbandlike feature. The choice of the downfolded Ru- d basis, of course, misses the features at higher binding energies, arising out of oxygen-dominated states. The downfolded LDA DOS in the effective Ru- d basis, as expected, does not show the Hubbard-like feature seen in PES data.

In the next step, we computed the full \mathbf{k} -resolved spectral function $A(\mathbf{k}, \omega)$ for the up- and down-spin channels of the ferromagnetically ordered SRO and for CRO. Figure 4 shows the result in comparison to the LDA band structure. The sharp quasiparticle peaks observed in the \mathbf{k} -integrated spectral function, shown in Fig. 3, are clearly visible on these intensity plots, and fairly well defined. They lie in the region from -0.5 to about 0.1 eV. At high energy, the e_g manifold becomes diffuse. The presence of the lower Hubbard band in the energy range 2–3 eV is also seen, giving rise to a picture of a correlated metal. Comparing this with the LDA band structure, first of all we notice the shifting of the correlated, complex band structure due to redistribution of spectral weights. We further notice a strong renormalization of the t_{2g} - e_g crystal field splitting (Δ) compared to LDA values as well as a bandwidth reduction given by Z_s . The renormalization of the crystal field splitting may be expressed as $\Delta_{\text{eff}} = \Delta_{\text{LDA}} + \text{Re}\Sigma_{e_g}(0) - \text{Re}\Sigma_{t_{2g}}(0)$. Interestingly, for the choice of $U = 3.5$ eV, for SRO, the renormalization given by, $\text{Re}\Sigma_{e_g}(0) - \text{Re}\Sigma_{t_{2g}}(0)$ is found to be negative and large (-1.54 eV) for the up-spin channel

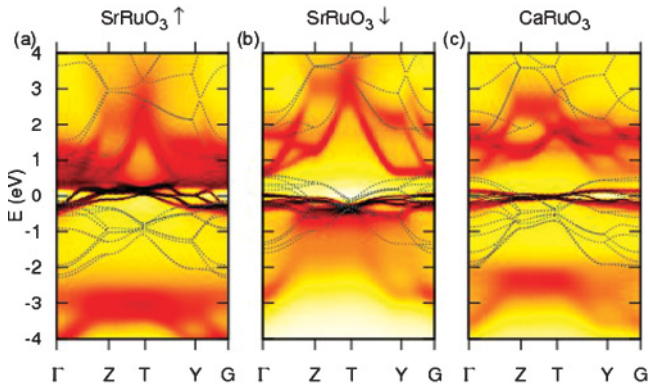


FIG. 4. (Color online) Intensity plot of the \mathbf{k} -resolved spectral function $A(\mathbf{k}, \omega)$ calculated by LDA+DMFT. The LDA band structure, shown with dots, has been superimposed for comparison.

but positive and small (0.4 eV) for the down-spin channel. For CRO, it is found to be negative as well, with a value of 0.7 eV.

Finally, in Fig. 5, we present the temperature evolution of m^* for SRO and CRO. The low-temperature values are essentially the same as those presented in Fig. 2. As temperature is increased, the m^* s deviate from their saturation values at some temperatures. Considering the fact that the deviation from the saturation value of m^* would indicate a deviation from pure FL behavior, one would expect a coherence temperature of about 900 K for SRO and about 550 K for CRO. Considering the contribution of t_{2g} electrons, the coherence temperature of CRO is further reduced to less than 400 K. This might explain

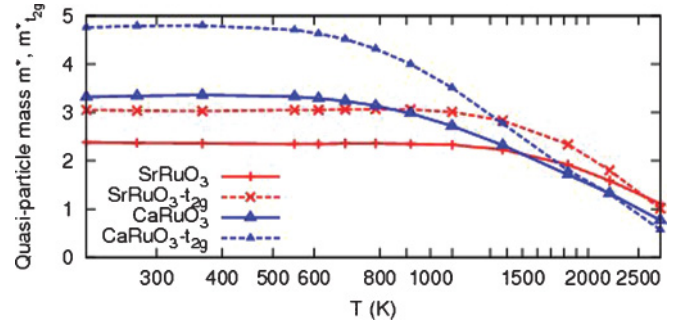


FIG. 5. (Color online) The temperature evolution of the mass enhancement factors for SRO and CRO.

the observation of non-FL-like behavior in the case of CRO and not in the case of SRO.²¹

In summary, we have carried out a DMFT study of the perovskite ruthenates SRO and CRO by solving the multi-orbital Hubbard Hamiltonian defined in an NMTO-constructed effective Ru- d Wannier basis. Our calculations show both SRO and CRO to be correlated metals with reasonably high mass enhancements. The coherence temperature for CRO is found to be substantially lower than that for SRO, providing a possible explanation for the observed non-FL-like behavior in CRO and its absence in SRO. The calculated spectral function is found to be in reasonable agreement with measured PES data. Our calculated \mathbf{k} -resolved spectral functions can be compared with future ARPES data. Our entire study does not include the effect of spin-orbit coupling. However, previous electronic-structure calculations⁸ have indicated that spin-orbit coupling does not have a large effect on the electronic structure.

¹G. Cao, S. McCall, M. Shepard, J. E. Crow, and R. P. Guertin, *Phys. Rev. B* **56**, 321 (1997).

²L. Klein, L. Antognazza, T. H. Geballe, M. R. Beasley, and A. Kapitulnik, *Phys. Rev. B* **60**, 1448 (1999).

³D. Toyota *et al.*, *Appl. Phys. Lett.* **87**, 162508 (2005).

⁴R. S. Singh, V. R. R. Medicherla, and Kalobaran Maiti, *Appl. Phys. Lett.* **91**, 132503 (2007); J. Park, S. J. Oh, J. H. Park, D. M. Kim, and C. B. Eom, *Phys. Rev. B* **69**, 085108 (2004).

⁵P. B. Allen, H. Berger, O. Chauvet, L. Forro, T. Jarlborg, A. Junod, B. Revaz, and G. Santi, *Phys. Rev. B* **53**, 4393 (1996).

⁶J. S. Ahn, J. Bak, H. S. Choi, T. W. Noh, J. E. Han, Y. Bang, J. H. Cho, and Q. X. Jia, *Phys. Rev. Lett.* **82**, 5321 (1999).

⁷I. I. Mazin and D. J. Singh, *Phys. Rev. B* **56**, 2556 (1997); D. J. Singh, *J. Appl. Phys.* **79**, 4818 (1996); K. Maiti, *Phys. Rev. B* **73**, 235110 (2006).

⁸J. M. Rondinelli, N. M. Caffrey, S. Sanvito, and N. A. Spaldin, *Phys. Rev. B* **78**, 155107 (2008).

⁹H. T. Jeng, S. H. Lin, and C. S. Hsue, *Phys. Rev. Lett.* **97**, 067002 (2006).

¹⁰A. Georges, G. Kotliar, W. Krauth, and M. J. Rozenberg, *Rev. Mod. Phys.* **68**, 13 (1996).

¹¹M. Shikano, T. K. Huang, Y. Inaguma, M. Itoh, and T. Nakamura, *Solid State Commun.* **90**, 115 (1994).

¹²E. Pavarini, A. Yamasaki, J. Nuss, and O. K. Andersen, *New J. Phys.* **7**, 188 (2005).

¹³M. V. Rama Rao, V. G. Sathe, D. Sornadurai, B. Panigrahi, and T. Shripathi, *J. Phys. Chem. Solids* **62**, 797 (2001).

¹⁴O. K. Andersen and T. Saha-Dasgupta, *Phys. Rev. B* **62**, R16219 (2000), and references therein.

¹⁵S. Sugano, Y. Tanabe, and N. Kamimura, *Multiplets of Transition-Metal Ions in Crystals*, series in Pure and Applied Physics (Academic Press, New York, 1970), Vol. 33.

¹⁶The choice of $J = U/2$ has been tested by considering a more realistic value of $J = 1$ eV. The results for physical quantities such as m^* were found to show a modest change of 3%.

¹⁷E. Jakobi, Ph.D. thesis, University of Mainz, 2010 [<http://ubm.opus.hbz-nrw.de/volltexte/2010/2275/>].

¹⁸A. Martin-Rodero, M. Baldo, F. Flores, and R. Pucci, *Solid State Commun.* **44**, 911 (1982); M. Potthoff, T. Wegner, and W. Nolting, *Phys. Rev. B* **55**, 16132 (1997).

¹⁹H. Kajueter and G. Kotliar, *Phys. Rev. Lett.* **77**, 131 (1996).

²⁰A. Callaghan, C. W. Moeller, and R. Ward, *Inorg. Chem.* **5**, 1572 (1966); J. M. Longo, P. M. Raccach, and J. B. Goodenough, *J. Appl. Phys.* **39**, 1327 (1968); A. Kanbayasi, *J. Phys. Soc. Jpn.* **44**, 108 (1978).

²¹P. Khalifah, I. Ohkubo, H. M. Christen, and D. G. Mandrus, *Phys. Rev. B* **70**, 134426 (2004); Y. S. Lee, J. Yu, J. S. Lee, T. W. Noh, T. H. Gimm, Han-Yong Choi, and C. B. Eom, *ibid.* **66**, 041104(R) (2002).